On the dielectric dispersion and absorption in nanosized manganese zinc mixed ferrites



2009 J. Phys.: Condens. Matter 21 146006

(http://iopscience.iop.org/0953-8984/21/14/146006)

J. Phys.: Condens. Matter **21** (2009) 146006 (12pp) doi:10.1088/0953-8984/21/14/146006

# On the dielectric dispersion and absorption in nanosized manganese zinc mixed ferrites

**E Veena Gopalan[1], K A Malini[2], D Sakthi Kumar[3], Yasuhiko Yoshida[3], I A Al-Omari[4], S Saravanan[5] and M R Anantharaman[1]**

[1] Department of Physics, Cochin University of Science and Technology, Cochin-682 022, Kerala, India
[2] Department of Physics, Vimala College, Thrissur-680 009, Kerala, India
[3] Bio-Nano Electronics Research Centre, Department of Applied Chemistry, Toyo University, Kawagoe, Saitama-350-8585, Japan
[4] Department of Physics, College of Science, P O Box 36, Sultan Qaboos University, PC 123, Muscat, Sultanate of Oman
[5] Department of Materials Engineering, Indian Institute of Science, Bangalore-560 012, India

E-mail: mraiyer@gmail.com

Received 10 November 2008, in final form 9 February 2009
Published 13 March 2009
Online at stacks.iop.org/JPhysCM/21/146006

**Abstract**

The temperature and frequency dependence of dielectric permittivity and dielectric loss of nanosized $Mn_{1-x}Zn_xFe_2O_4$ (for $x = 0, 0.2, 0.4, 0.6, 0.8, 1$) were investigated. The impact of zinc substitution on the dielectric properties of the mixed ferrite is elucidated. Strong dielectric dispersion and broad relaxation were exhibited by $Mn_{1-x}Zn_xFe_2O_4$. The variation of dielectric relaxation time with temperature suggests the involvement of multiple relaxation processes. Cole–Cole plots were employed as an effective tool for studying the observed phenomenon. The activation energies were calculated from relaxation peaks and Cole–Cole plots and found to be consistent with each other and indicative of a polaron conduction.

(Some figures in this article are in colour only in the electronic version)

## 1. Introduction

Ferrites are ferrimagnetic oxides and are important magnetic materials, widely used in a number of devices like transformer cores, microwave antennas and magnetic recording devices [1, 2]. With the advent of nanotechnology there is renewed interest in ferrites since many of the useful properties of these materials can be modified suitably [3, 4]. The finite size effects in the nanoregime can be employed to tailor structural, magnetic and electrical properties of nanostructured ferrites. In the nanoregime altogether different mechanisms are responsible for the modified properties.

Manganese ferrite in the micron regime is found to be 20% inverse with a stoichiometry of $Mn_{0.8}Fe_{0.2}[Mn_{0.2}Fe_{0.8}]O_4$, where cations in brackets occupy the octahedral sites [5]. A higher inversion up to 60% has been reported in nanosized manganese ferrites [6]. When zinc is substituted for manganese in $Mn_{1-x}Zn_xFe_2O_4$, the zinc ions are expected to occupy the tetrahedral sites. In coarser sized samples of manganese zinc ferrite, zinc ($Zn^{2+}$) ions were found to exist only on the tetrahedral sites (A sites) as expected. However, zinc is found to occupy the octahedral sites of nanosized manganese zinc ferrites prepared by co-precipitation methods, the reverse micellar method, the pulsed laser deposition method or the high energy ball milling method [7, 8]. The occupancy of zinc ions in octahedral sites in the nanoregime can alter the cation distribution to a great extent and this will modify the structural and magnetic properties in the case of $Mn_{1-x}Zn_xFe_2O_4$ nanoparticles.

Nanoparticles of a series belonging to $Mn_{1-x}Zn_xFe_2O_4$ (where $x = 0.0, 0.2, 0.4, \ldots, 1$) were found to exhibit different structural and magnetic properties with respect to their bulk counterparts. A reduction in lattice parameter, accompanied by reduced magnetization values, enhanced

 

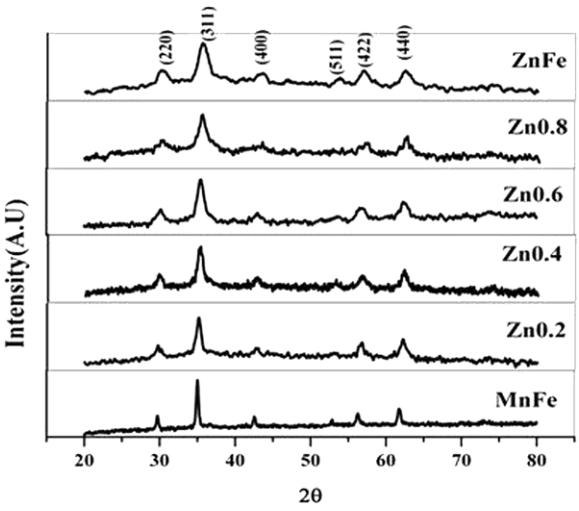


**Figure 1.** XRD patterns of $Mn_{1-x}Zn_xFe_2O_4$.

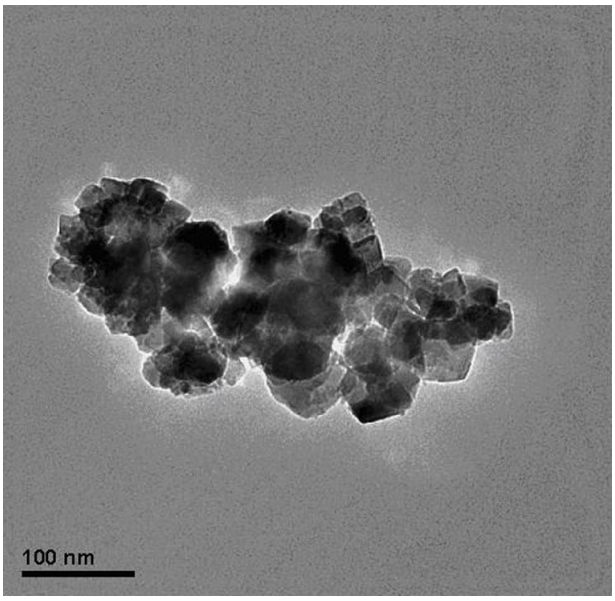


**Figure 2.** TEM image of $MnFe_2O_4$.

Curie temperature and a metastable cation distribution, are all hall marks of nanosized manganese zinc ferrites [9].

The dielectric permittivity of ceramic materials is found to depend on the frequency of measurement. It decreases from static permittivity ($\varepsilon_s$) at low frequencies to a smaller limiting value of $\varepsilon_\alpha$ at higher frequencies. This has been explained by Debye [10]; the difference in the values of $\varepsilon_s$ and $\varepsilon_\alpha$ has been attributed to dipolar polarization and generally a single relaxation time is associated with the dielectric relaxation. In real dielectrics, different types of dipole species are present and these may give rise to several relaxation times instead of a single one. Hence Cole and Cole modified Debye's equations to incorporate the effects of multiple relaxation time. These Cole–Cole plots based on these modified equations can be effectively used for studying the dielectric relaxation at the molecular level and for evaluation of the dispersion parameters [11].

Dispersion and absorption can also occur in inhomogeneous dielectrics like ferrites. In ferrites, the dielectric properties are explained assuming that a heterogeneous structure consisting of grains and grain boundaries exist [12–14]. Dielectric relaxation was reported in micron sized particles in the frequency regime of 1–100 kHz. Dielectric dispersion and dielectric relaxation were found to change with grain size. In the case of nanometer sized particles the existence of a large number of interface dipoles can give rise to different relaxation processes, resulting in a broader relaxation. Sharp dispersion and a relaxation effect with multiple relaxation times are reported in ferrites in the nanoregime [15]. Dielectric properties are expected to be modified substantially because of the presence of nanosized grains and grain boundaries.

In ferrites the mechanism of dielectric polarization was found to be similar to the electrical conduction mechanism [16]. In the case of manganese zinc ferrites, electron hopping between $Fe^{3+} \leftrightarrow Fe^{2+}$ ions and hole hopping between $Mn^{2+} \leftrightarrow Mn^{3+}$ ions are found to be responsible for electrical conductions [17]. In micron sized particles prepared by solid state reactions, sintering gives rise to $Fe^{2+}$ and $Mn^{3+}$ ions. However in the nanoregime, where no high temperature sintering is involved, the presence of $Fe^{2+}/Fe^{3+}$ and $Mn^{3+}/Mn^{2+}$ will be dependent on the preparative conditions. A cation redistribution which is different from that of their bulk cousins is observed in nanoparticles of ferrite [8]. These factors are bound to play a major role in deciding the overall dielectric properties of the nanosized manganese zinc ferrite [15].

It is in this context that a detailed investigation on the dielectric properties of a series belonging to $Mn_{1-x}Zn_xFe_2O_4$ assumes significance. The employment of a Cole–Cole plot to evaluate various parameters, namely, $\varepsilon_s$ (static dielectric constant), $\varepsilon_0$ (optical dielectric constant), $\alpha$ (spreading factor), $\tau_0$ (average relaxation time) and $\tau$ (molecular relaxation time), will definitely lead to an understanding of the phenomenon of dispersion occurring in the nanosized mixed ferrites. In this investigation manganese zinc ferrites belonging to the series $Mn_{1-x}Zn_xFe_2O_4$ (for $x = 0$, 0.2, 0.4, 0.6, 0.8 and 1) are synthesized by employing low temperature methods. In order to gain an insight into the phenomenon of dielectric dispersion and absorption, the dielectric properties of the ferrites in the frequency regime of 100 kHz–8 MHz are evaluated and the results are correlated.

## 2. Experimental details

Mixed ferrites belonging to $Mn_{1-x}Zn_xFe_2O_4$ ($x = 0$ to 1 in steps of $x = 0.2$) were synthesized by the wet chemical co-precipitation technique under identical conditions. Aqueous solutions of $(1-x)$ molar manganese chloride ($MnCl_2{\cdot}4H_2O$) and $x$ molar zinc chloride ($ZnCl_2{\cdot}$anhydrous) and a 2 M solution of ferric chloride($FeCl_3{\cdot}$anhydrous) were mixed to form a solution and the solution was poured quickly into boiling 10 M NaOH solution diluted in 1800 ml of water under vigorous stirring. The pH and the temperature were maintained at 12.5–13 and 90 °C respectively. The precipitate was washed

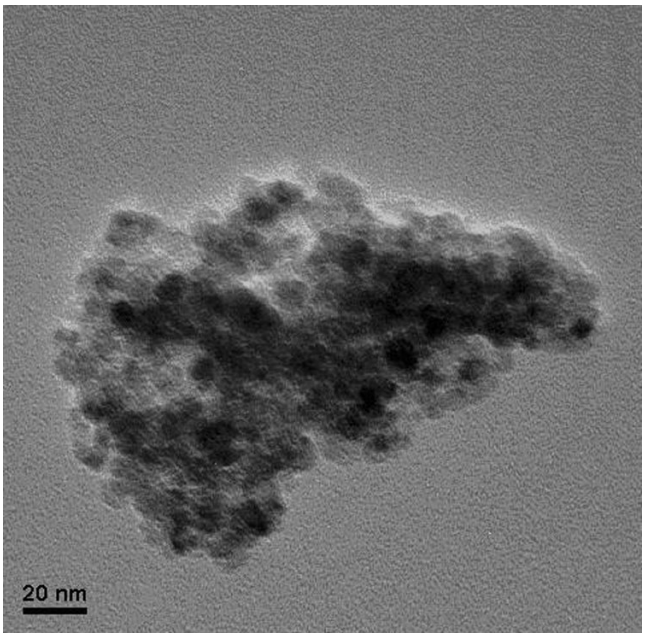


**Figure 3.** TEM image of $ZnFe_2O_4$.

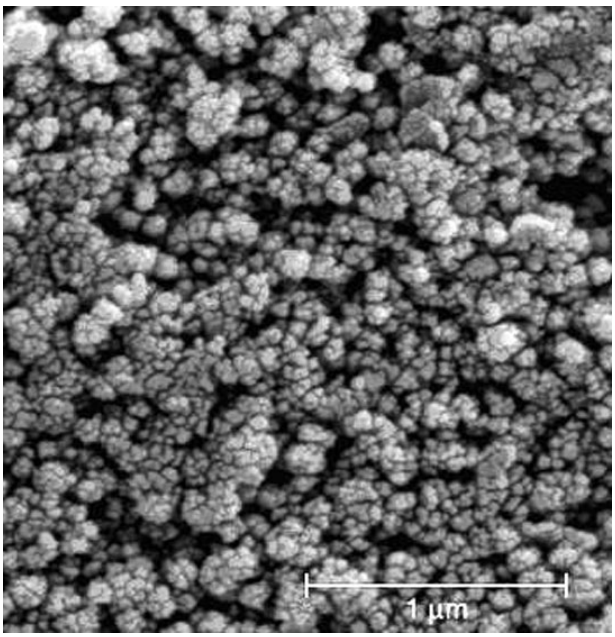


**Figure 4.** SEM image of $MnFe_2O_4$.

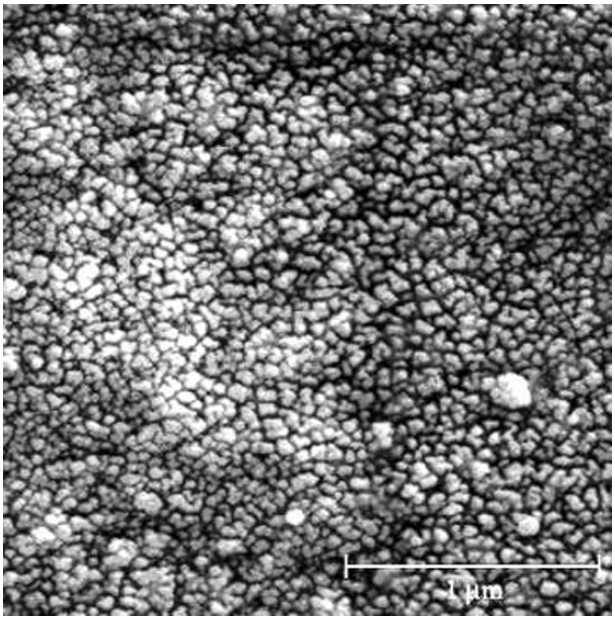


**Figure 5.** SEM image of $MnZnFe_2O_4$.

several times with distilled water, then filtered and dried in an oven.

X-ray diffraction patterns of the samples were recorded using an x-ray powder diffractometer (Rigaku Dmax-C) using Cu K$\alpha$ radiation ($\lambda = 1.5405$ Å). Lattice parameters of the compositions were calculated assuming cubic symmetry and the average crystallite size of each sample was estimated by employing the Debye–Scherrer formula [18]. The particle sizes of samples were also evaluated from transmission electron microscopy (TEM) measurements (Jeol JEM-2200 FS). Magnetic hysteresis loop parameters at room temperature were evaluated by using a vibrating sample magnetometer (DMS 1660 VSM). Scanning electron microscopy was employed to check the morphology of the samples (JSM-6335 FESEM).

Dielectric measurements were carried out using a home made dielectric cell and an HP 4285 *LCR* meter in the frequency range of 100 kHz–8 MHz over a temperature range of 303–393 K. The data acquisition was automated by interfacing the *LCR* meter with a virtual instrumentation package called LABVIEW (National Instruments). Cole–Cole plots at different temperatures were drawn by the circle least square method utilizing the real and imaginary values of dielectric permittivity [19] to derive dispersion parameters.

The relative dielectric permittivity $\varepsilon$ of the sample was calculated using the relation

$$C = \frac{\varepsilon_r \varepsilon_0 A}{d} \tag{1}$$

where $C$ is the capacitance of the parallel plate capacitor with thickness $d$ and area of cross-section $A$, $\varepsilon_0$ the permittivity of free space and $\varepsilon_r$ is the relative dielectric permittivity of the material, hereafter termed as the dielectric permittivity $\varepsilon$.

The loss factor or dissipation factor in any dielectric is given by the expression

$$\tan\delta = \frac{\varepsilon''(\omega)}{\varepsilon'(\omega)} \tag{2}$$

where $\varepsilon'$ and $\varepsilon''$ are the real and imaginary parts of the complex dielectric permittivity respectively.

The Debye equation for dielectric dispersion can be written in the form

$$\varepsilon^* - \varepsilon_\infty = \frac{(\varepsilon_s - \varepsilon_\infty)}{(1 + j\omega\tau)} \tag{3}$$

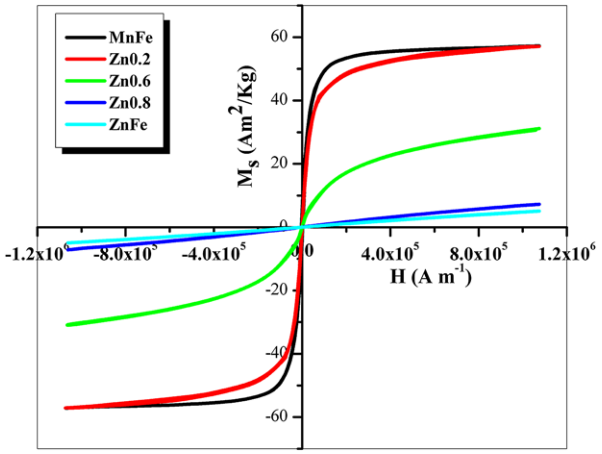


**Figure 6.** Room temperature hysteresis curves of $Mn_{1-x}Zn_xFe_2O_4$.

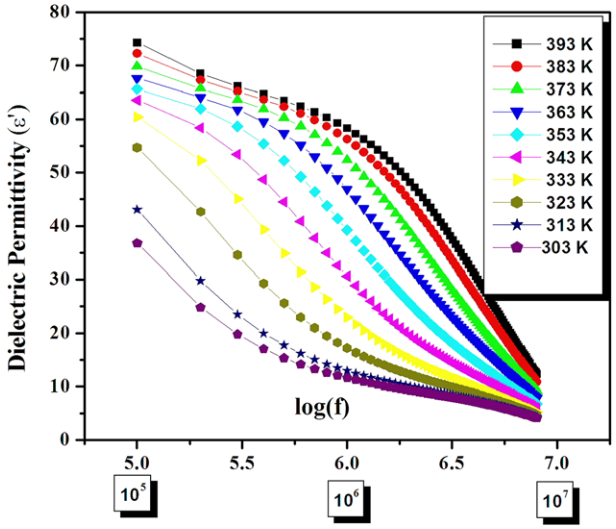


**Figure 7.** $\varepsilon'$ versus log $f$ in $MnFe_2O_4$.

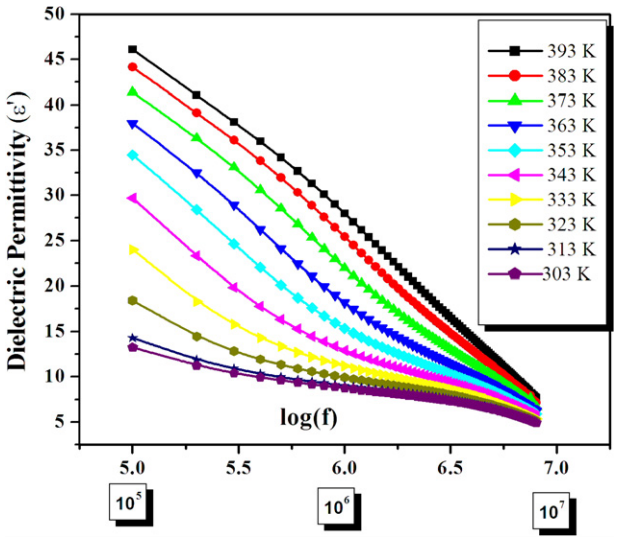


**Figure 8.** $\varepsilon'$ versus log $f$ in $Mn_{0.6}Zn_{0.4}Fe_2O_4$.

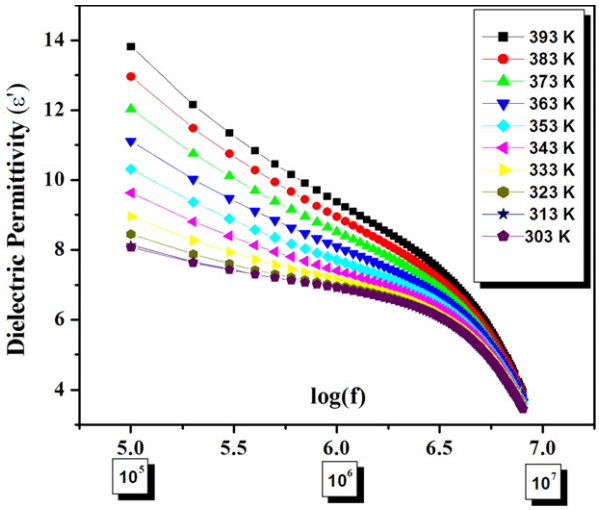


**Figure 9.** $\varepsilon'$ versus log $f$ in $Mn_{0.8}Zn_{0.2}Fe_2O_4$.

where $\varepsilon_s$ and $\varepsilon_\alpha$ are the limiting frequencies, i.e. the static dielectric constant and optical dielectric constant, $\omega = 2\pi f_{max}$ and $\tau$ is the molecular relaxation time. Cole and Cole modified the Debye equation of dielectric dispersion considering the existence of multiple relaxation time [20–22]. In this case the permittivity follows the empirical equation

$$\varepsilon^* - \varepsilon_\infty = \frac{(\varepsilon_s - \varepsilon_\infty)}{1 + (j\omega\tau_0)^{1-\alpha}} \quad (4)$$

where $\tau_0$ is the average relaxation time; $\alpha$ the spreading factor of the actual relaxation time $\tau$ about its mean value $\tau_0$ and $\alpha$ lies in the range 0–1. A plot of $\varepsilon''$ for a certain frequency against $\varepsilon'$ at the same frequency in the complex plane is called a Cole–Cole plot. For a dielectric with a single relaxation time, the Cole–Cole plot is a semicircle. For $\alpha > 0$, the Cole–Cole plot is a circular arc with its center lying below the real axis. The spreading factor, average relaxation time $\tau_0$ and molecular relaxation time $\tau$ can be estimated from the Cole–Cole equation. A detailed description of these derivations is given elsewhere [22].

## 3. Results and discussion

### *3.1. Structural and magnetic characterization*

The x-ray diffraction patterns of mixed ferrites belonging to the series $Mn_{1-x}Zn_xFe_2O_4$ are depicted in figure 1. They are found to be characteristic of a spinel structure. The particle size and lattice constant are evaluated and are shown in table 1.

Further the particle sizes were also estimated using TEM and were found to be in good agreement with those obtained from the line broadening analysis of x-ray diffraction. The reduction of particle size with zinc substitution is clearly evident from the TEM images (figures 2 and 3). Scanning electron micrographs of the samples are depicted in figures 4 and 5. The micrographs show the presence of a large number of interfaces, which have a direct bearing on the dielectric properties of these ferrites.

Representative hysteresis loops for $Mn_{1-x}Zn_xFe_2O_4$ at room temperature are portrayed in figure 6. The magnetization

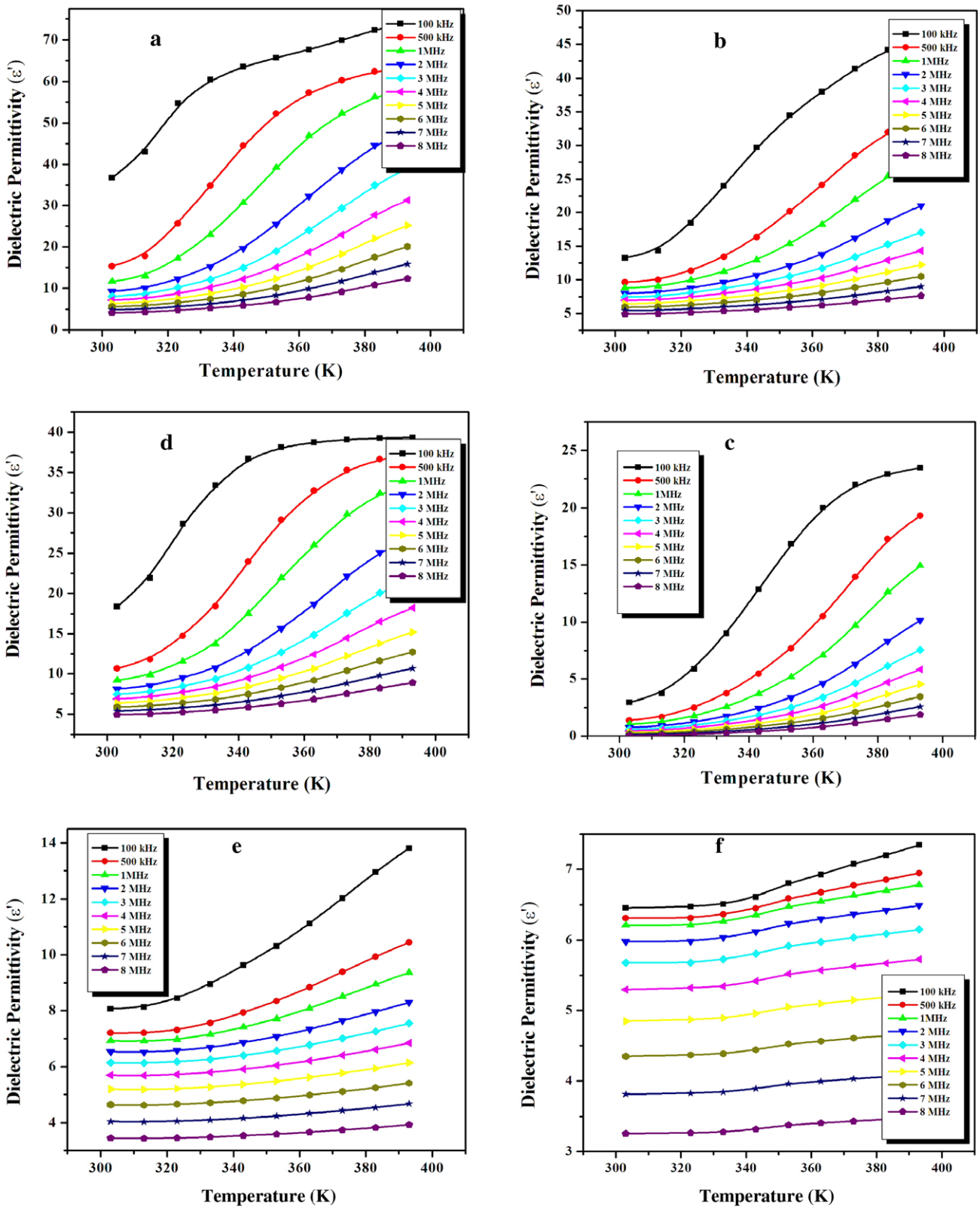


**Figure 10.** (a)–(f) $\varepsilon'$ versus temperature in $Mn_{1-x}Zn_xFe_2O_4$: (a) $MnFe_2O_4$, (b) Zn0.2, (c) Zn0.4, (d) Zn0.6, (e) Zn0.8, (f) ZnFe.

values are tabulated and shown in table 1. The magnetic properties of nanosized $Mn_{1-x}Zn_xFe_2O_4$ do not comply with those of the same ferrite prepared in the micron regime. The magnetic properties were found to be different from their bulk counterparts [23]. The deviations from the corresponding bulk values proclaim the existence of a different cation distribution, which can give rise to different exchange interactions and will be manifested in the form of modified magnetic properties.

**Table 1.** Structural and magnetic properties of $Mn_{1-x}Zn_xFe_2O_4$.

| $Mn_{1-x}Zn_xFe_2O_4$ ($x$) | Particle size (nm) | Lattice parameter (Å) | Maximum magnetization at 300 K (A $m^2$ $kg^{-1}$) |
|---|---|---|---|
| 0 | 29.1 | 8.497 | 57 |
| 0.2 | 14.7 | 8.471 | 56 |
| 0.4 | 12.9 | 8.454 | 53 |
| 0.6 | 10.3 | 8.398 | 31 |
| 0.8 | 8.2 | 8.354 | 7.5 |
| 1 | 7.2 | 8.414 | 5.2 |

### 3.2. *Frequency and temperature dependence*

*3.2.1. Dielectric dispersion.* The variation of dielectric properties with frequency is depicted in figures 7–9. It can be seen that the relative dielectric permittivity, $\varepsilon$, exhibits an inverse dependence on frequency as reported in a number of ferrite compounds. It decreases with increase in frequency and remains a constant at higher frequencies. In our frequency regime of measurements (100 kHz–8 MHz), it is the polarization due to interface dipoles which contributes to the overall dielectric properties of the sample [24, 25].

Earlier, theories like the Maxwell–Wagner theory of dielectric dispersion were employed to study the dispersion [12, 13]. It is assumed that the dielectric polarization had its origin in the heterogeneous structure of ferrites with grains and grain boundaries [26]. The effect of grain interfaces is more pronounced at lower frequencies, where we observe relatively large values of $\varepsilon'$. The space charge polarization occurring at the interfaces at lower frequencies can also contribute to dielectric permittivity at lower frequencies.

Many researchers have reported a similarity between the conduction process and dielectric polarization in ferrites [15]. Normally, for manganese zinc ferrites, the conduction process is explained on the basis of electron hopping between $Fe^{2+}$ and $Fe^{3+}$ and hole hopping between $Mn^{2+}$ and $Mn^{3+}$ on the octahedral sites. In the Rezlescue model, the hopping of electrons/holes results in the local displacements of the electrons/holes which collectively contribute to the total polarization [27]. Denecke *et al* observed the presence of $Mn^{3+}$ ions in octahedral sites in co-precipitated manganese zinc ferrite nanoparticles prepared using highly basic solution [28]. The electrons exchanging between $Fe^{2+}$ and $Fe^{3+}$ ions and the holes that transfer between $Mn^{3+}$ and $Mn^{2+}$ ions are responsible for electric conduction and dielectric polarization in manganese zinc ferrites. At higher frequencies, the frequency of electron/hole exchange will not be able to follow the applied electric field, thus resulting in a decrease in polarization. Consequently, the dielectric permittivity attains a constant value.

The temperature dependence of $\varepsilon'$ at selected frequencies is shown in figures 10(a)–(f). As the temperature increases the orientation of interface dipoles is facilitated and this enhances the dielectric permittivity. At lower frequencies the rapid increase in dielectric constant with temperature is mainly due to polarization due to interfacial dipoles which are strongly

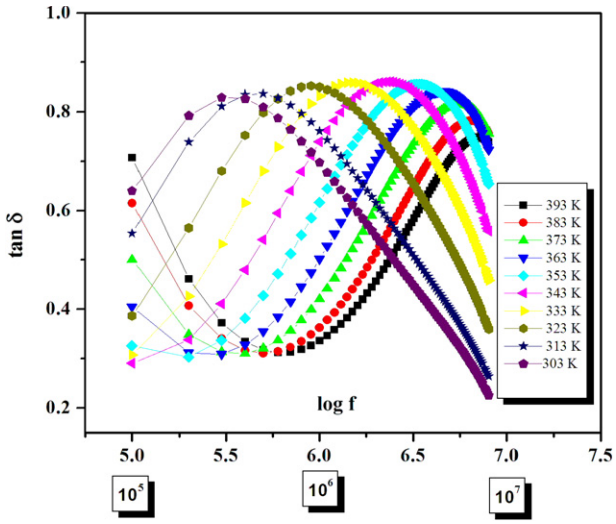


**Figure 11.** tan $\delta$ versus log $f$ in $MnFe_2O_4$.

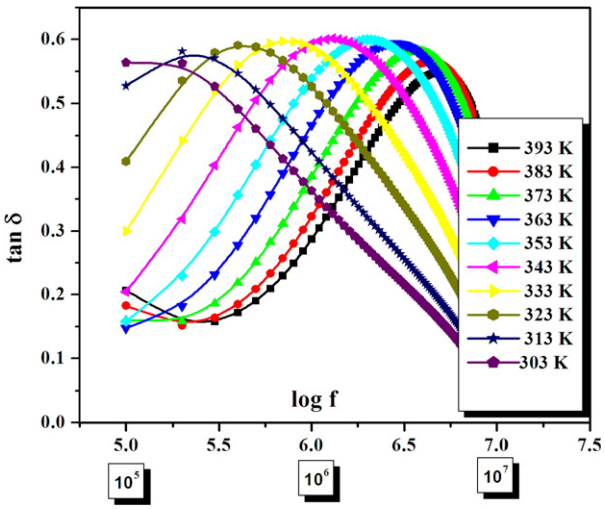


**Figure 12.** tan $\delta$ versus log $f$ in $Mn_{0.2}Zn_{0.8}Fe_2O_4$.

dependent on temperature [25]. As temperature increases, the accumulation of charges on the grain boundaries increases, which causes an increase in the interfacial polarization. This is at lower frequencies. Therefore, the dielectric polarization increases, resulting in an increase of $\varepsilon'$ with temperature at lower frequencies.

*3.2.2. Dielectric absorption.* Dielectric absorption in a material is characterized by tan $\delta$ and dielectric loss ($\varepsilon''$) values. It can be seen that tan $\delta$ and $\varepsilon''$ values when plotted against frequency exhibit relaxations at specific frequencies and temperatures (figures 11–17). Dielectric relaxation occurs when the hopping frequency of charge carriers is equal to the frequency of the applied field [29]. However, it is to be noted that a relaxation can be noticed in the case of manganese rich compositions, while for the zinc rich compositions the relaxation is found to be absent (figures 15 and 18). This may be due to the reduction in number of hopping charges available

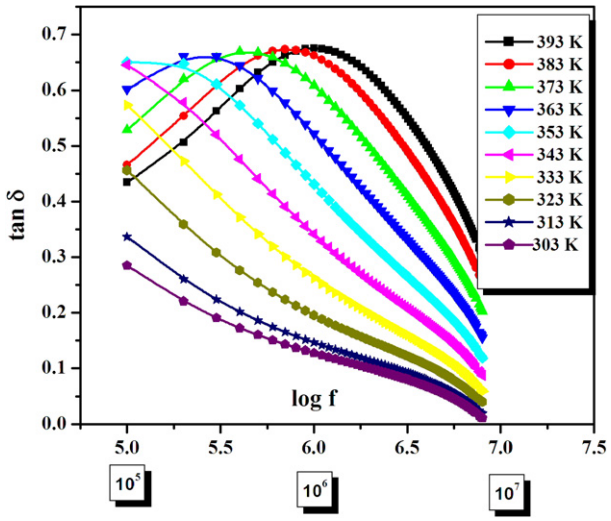


**Figure 13.** tan $\delta$ versus log $f$ in $Mn_{0.4}Zn_{0.6}Fe_2O_4$.

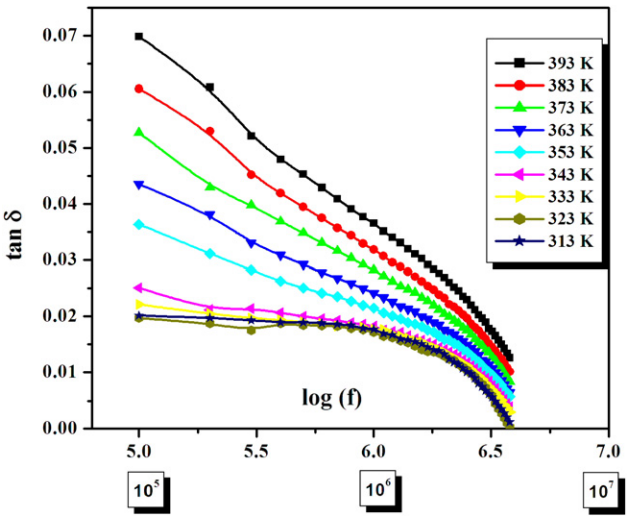


**Figure 14.** tan $\delta$ versus log $f$ in $ZnFe_2O_4$.

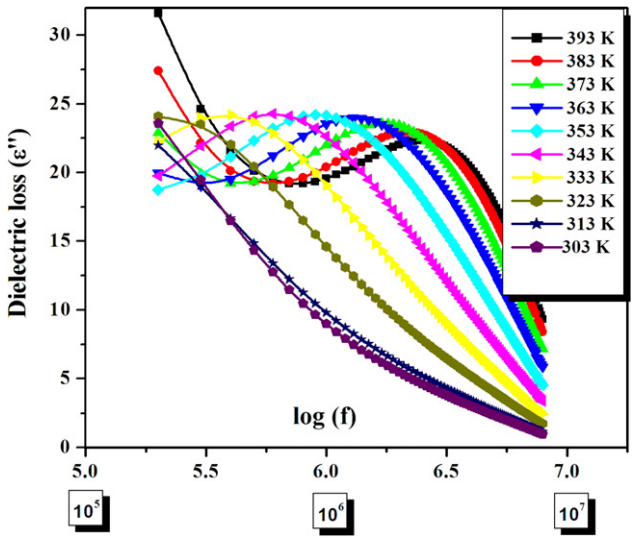


**Figure 15.** $\varepsilon''$ versus log $f$ in $MnFe_2O_4$.

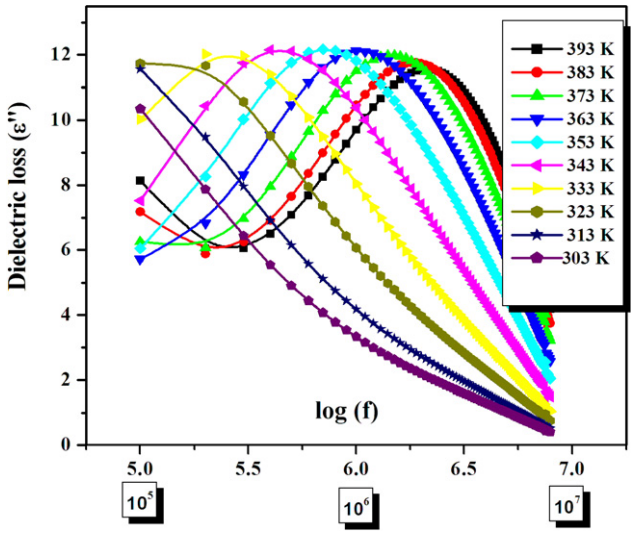


**Figure 16.** $\varepsilon''$ versus log $f$ in $Mn_{0.8}Zn_{0.2}Fe_2O_4$.

for hopping as the zinc concentration increases. There also is a likelihood that the relaxation peaks corresponding to these compositions lie outside the frequency range of measurement.

### *3.3. Effect of zinc substitution on dielectric properties*

The zinc substitution has a direct influence in modifying the dielectric characteristics. The variation of $\varepsilon$ with zinc compositions is studied for different temperatures and different frequencies (figures 18 and 19).

The dielectric permittivity decreases with increase in zinc content. With increasing zinc content there is a decrease in manganese ions ($Mn^{3+}$) and consequently the presence of $Fe^{2+}$ ions in the octahedral sites is also reduced. Hence the number of $Mn^{3+}$–$Mn^{2+}$ and $Fe^{3+}$–$Fe^{2+}$ pairs available for hole and electron hopping will be smaller as we increase the zinc content. As a result hopping decreases and the charged species are accumulated at the grain boundaries. Therefore, the resistance of the grain boundaries increases and hence the probability for charged species to cross over the grain boundaries decreases. This will subsequently result in reduced hopping and dielectric polarization, which is manifested in low permittivity values in zinc rich compositions. Both at 100 kHz and 8 MHz a nominal increase of dielectric permittivity is noticed in compositions from $x = 0.8$ to zinc ferrite compared to the composition $x = 0.6$. These two samples were found to possess finer size and are found to be highly homogeneous. Hence an increase in dielectric constant can be attributed to a size induced effect in these compositions.

Figures 20 and 21 depict the effect of zinc substitution on the tan $\delta$ of the $Mn_{1-x}Zn_xFe_2O_4$ series. A reduction in dielectric absorption values is seen with an increase in zinc concentration. A decrease in the $Fe^{2+}/Fe^{3+}$ and $Mn^{2+}/Mn^{3+}$ pairs available for conduction with increase in zinc concentration can be thought of as one of the reasons for this type of behavior in manganese zinc ferrites.

We have suggested that the dielectric polarization can be explained based on the hopping of charge carriers. A

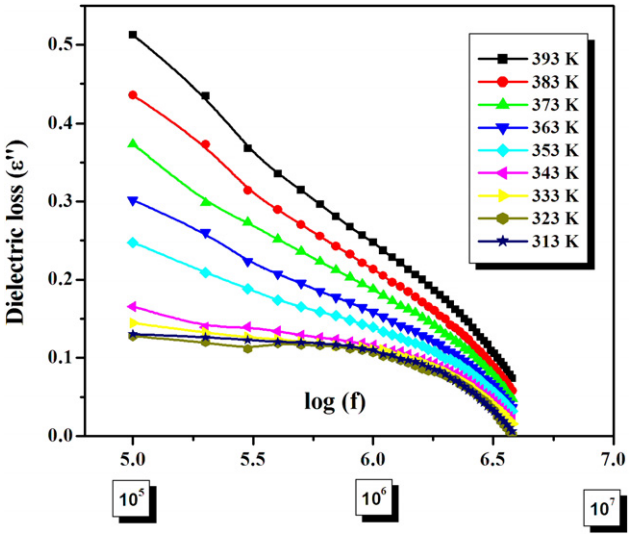


**Figure 17.** $\varepsilon''$ versus log $f$ in $ZnFe_2O$.

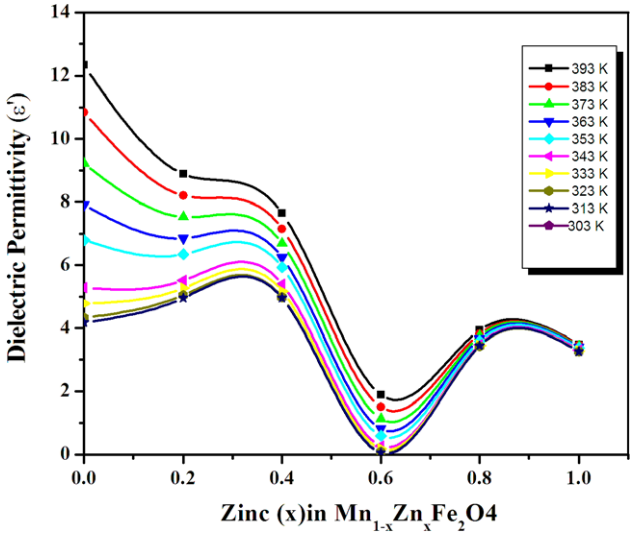


**Figure 19.** $\varepsilon'$ versus zinc content (at 8 MHz).

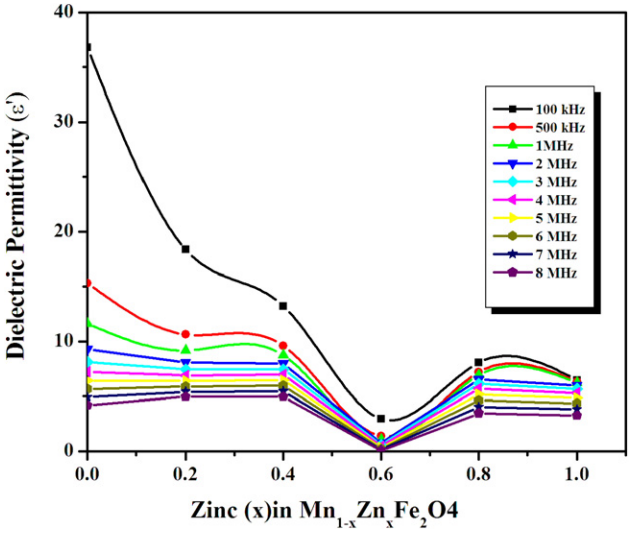


**Figure 18.** $\varepsilon'$ versus zinc content (at 303 K).

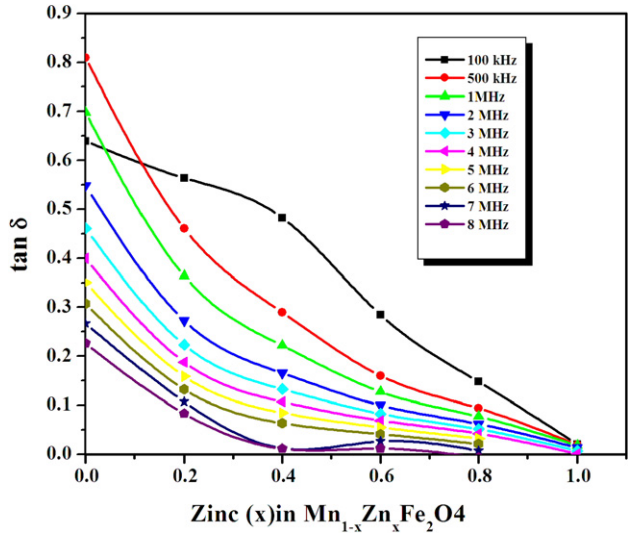


**Figure 20.** $\tan\delta$ versus zinc content (at 303 K).

relaxation occurs when the hopping frequency equals the applied frequency The evaluation of the activation energy can provide more insight on the transport properties of ferrites [30].

### *3.4. Calculation of activation energy from relaxation peaks*

The condition for observing a maximum in the dielectric loss of a dielectric material is given by the relation [29],

$$\omega\tau' = 1 \qquad \text{where } \tau' \text{ is the relaxation time and } \omega = 2\pi f_{\max}. \tag{5}$$

The value of $f_{\max}$ can easily be observed from figure 11. The relaxation time $\tau$ can be determined from (5). Then $\tau$ can be written as

$$\tau' = \tau_0 \exp\left(\frac{E_d}{k_B T}\right) \tag{6}$$

where $\tau_0$ is the pre-exponential constant, which equals the relaxation time at infinitely high temperatures, $k_B$ is the Boltzmann's constant, $T$ is the absolute temperature and $E_d$ the activation energy for dielectric relaxation. The variation of $\tau'$ with temperature is shown in figure 22, which shows a decrease in relaxation time with temperature. This points towards the possibility of existence of multiple relaxation mechanisms with a distribution of relaxation times in the nanosystem.

From the slope of the graph between $\ln\tau$ and $1000/T$, $E_d$, the activation energy for dielectric relaxation, can be determined (figure 23). The hopping depends on the activation energy, which is associated with the electrical energy barrier experienced by the electrons during hopping. Since $\tau = 1/2P$, where $P$ is the hopping probability, the decrease in relaxation time with temperature results in an increase in hopping probability with temperature.

The activation energy for dielectric relaxation for $MnFe_2O_4$, $Mn_{0.8}Zn_{0.2}Fe_2O_4$ and $Mn_{0.6}Zn_{0.6}Fe_2O_4$ is calculated and found to be 0.329 eV, 0.412 eV and 0.497 eV respectively. The large values of activation energy point

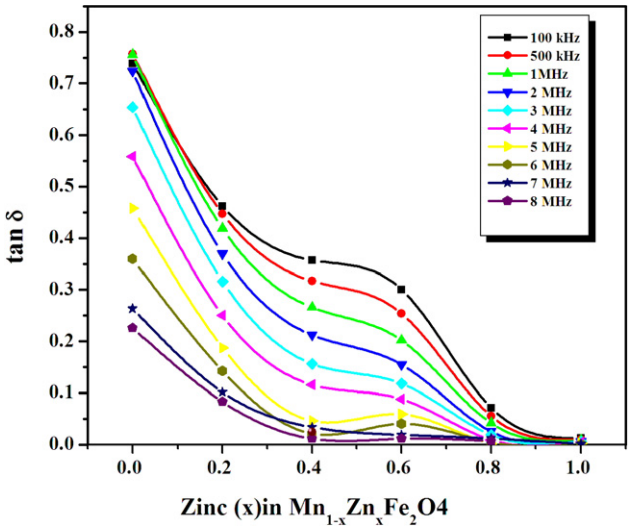


**Figure 21.** tan $\delta$ versus zinc content (at 8 MHz).

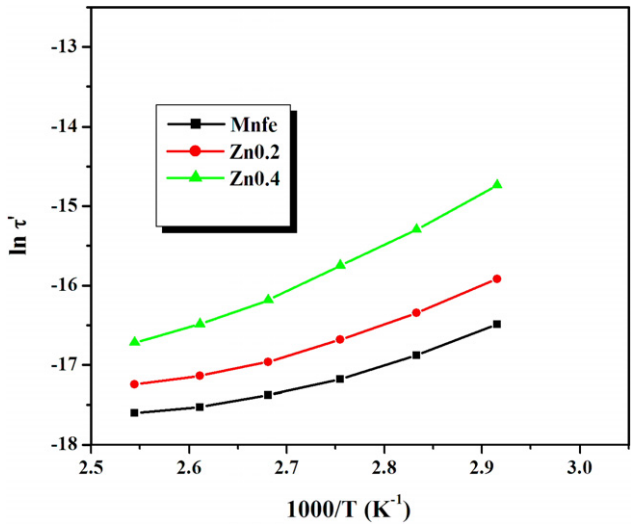


**Figure 23.** ln $\tau$ versus $1000/T\,(\mathrm{K}^{-1})$.

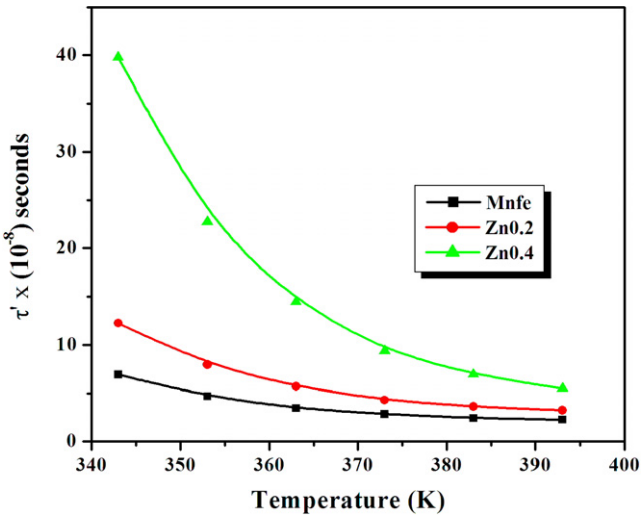


**Figure 22.** Relaxation time ($\tau$) versus temperature.

towards polaron hopping [31]. The observation of a relatively large value of activation energy and relaxation nature of dielectric loss suggests two distinct conduction processes, namely quantum mechanical tunneling through the barrier separating the two equilibrium positions and the classical hopping of a carrier over the barrier or some combination or a variant of the two [32, 33].

The presence of strong dielectric dispersion and broad relaxation peaks in the dielectric loss spectra is because of multiple relaxations. Therefore, Cole–Cole plots were employed as an effective tool for studying the observed phenomena [22]. A knowledge of dispersion parameters can help reveal the dynamics of the relaxation phenomena in these materials.

### *3.5. Cole–Cole representation of dielectric data*

The Cole–Cole plots corresponding to the compositions of $MnFe_2O_4$ and $Mn_{0.8}Zn_{0.2}Fe_2O_4$ were plotted, since a relaxation in $\varepsilon''$ was found to be absent for all compositions with $x$ greater than 0.2. They are shown in figures 24(a)–(c) and 25(a)–(c). From the Cole–Cole analysis, the dispersion parameters of these two compositions were evaluated. The dispersion parameters like $\varepsilon_s$ (static dielectric constant), $\varepsilon_\alpha$ (optical dielectric constant), $\alpha$ (spreading factor), $\tau_0$ (average relaxation time) and $\tau$ (molecular relaxation time) of the two

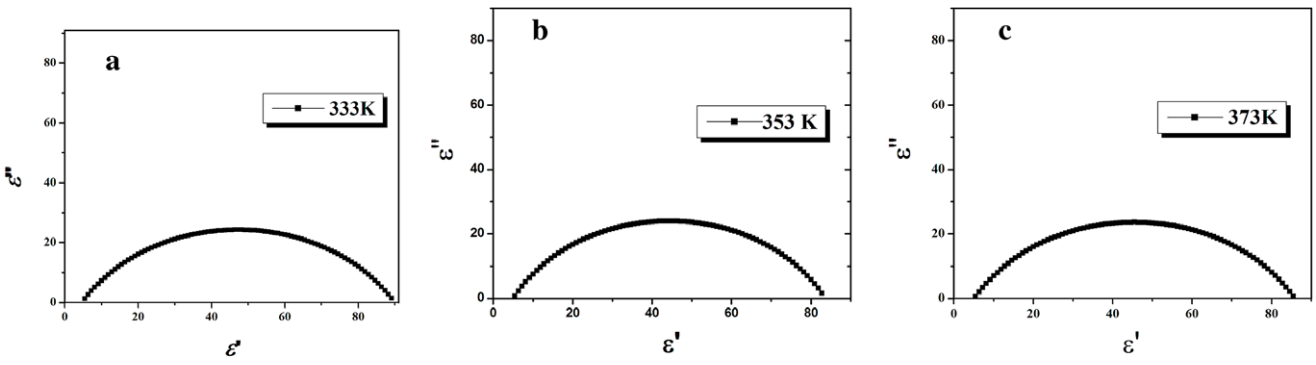


**Figure 24.** Cole–Cole plots of $MnFe_2O_4$: (a) 333 K, (b) 353 K and (c) 373 K.

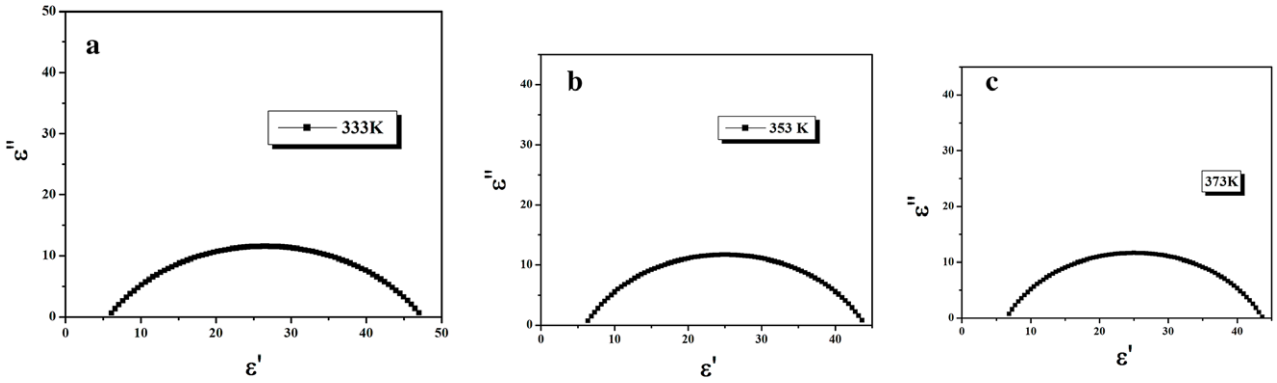


**Figure 25.** Cole–Cole plots of $Mn_{0.8}Zn_{0.2}Fe_2O_4$: (a) 333 K, (b) 353 K and (c) 373 K.

**Table 2.** Dispersion parameters from Cole–Cole analysis.

| | $\varepsilon_s$ | | $\varepsilon_\alpha$ | | $\alpha$ | | $\varepsilon''$ | | $\tau_0$ ($10^{-8}$ s) | | $\tau$ ($10^{-8}$ s) | |
|---|---|---|---|---|---|---|---|---|---|---|---|---|
| $T$ (K) | MnFe | Zn0.2 | MnFe | Zn0.2 | MnFe | Zn0.2 | MnFe | Zn0.2 | MnFe | Zn0.2 | MnFe | Zn0.2 |
| 373 | 85.85 | 43.75 | 6.41 | 5.16 | 0.326 | 0.289 | 24.28 | 11.66 | 3.43 | 2.70 | 1.86 | 2.45 |
| 363 | 84.02 | 43.83 | 6.11 | 5.12 | 0.308 | 0.293 | 24.10 | 11.69 | 5.04 | 3.47 | 2.39 | 3.59 |
| 353 | 83.62 | 44.05 | 6.02 | 5.06 | 0.302 | 0.299 | 23.99 | 11.67 | 6.95 | 4.82 | 3.31 | 4.95 |
| 343 | 85.67 | 45.12 | 5.78 | 4.85 | 0.314 | 0.324 | 23.84 | 11.56 | 10.96 | 6.63 | 4.55 | 7.77 |
| 333 | 89.97 | 47.43 | 5.65 | 4.67 | 0.341 | 0.357 | 23.61 | 11.54 | 17.41 | 8.60 | 5.88 | 12.23 |

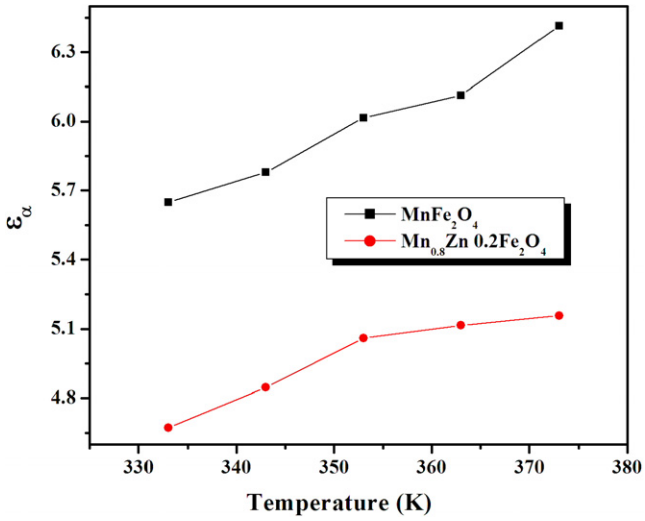


**Figure 26.** Variation of $\varepsilon_\alpha$ with temperature.

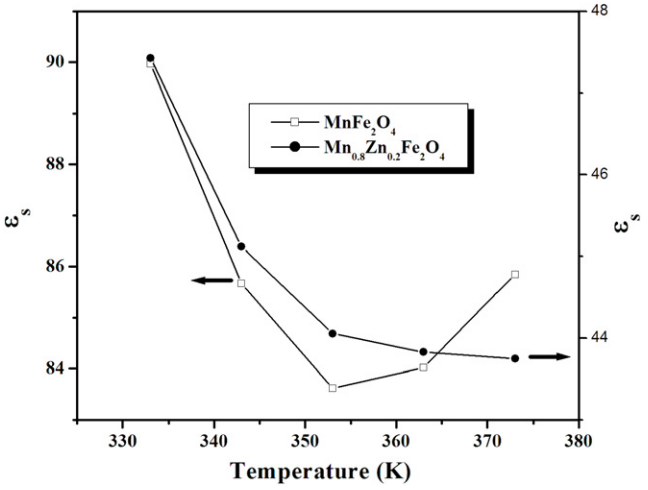


**Figure 27.** Variation of $\varepsilon_s$ with temperature.

samples are evaluated and they are tabulated and their variation with temperature analyzed.

The optical dielectric constant ($\varepsilon_\alpha$) is found to be increasing with temperature (figure 26), while the static dielectric constant is found to decrease (figure 27). However, the variation of the two limiting values of dielectric permittivity within the measured temperature range was not very large. The spreading factor is a measure of the broadening of the relaxation time (figure 28). The average relaxation time is the effective time constant for the relaxation involved, while the molecular or intrinsic relaxation time is the time constant for the immediate molecular dipole relaxation. Both average relaxation time and molecular relaxation time decrease with increasing temperature (table 2). The rise in temperature causes a reduction in the mean time of stay of ionic dipoles, resulting in a decrease of relaxation time with temperature. Hence, as relaxation time decreases with temperature, there is a decrease in spreading factor.

Activation energy for dielectric relaxation can be calculated from the slope of the $\ln\tau$ versus $1000/T$ plot (figure 29). The activation energies calculated for the $MnFe_2O_4$ and $Mn_{0.8}Zn_{0.2}Fe_2O_4$ are 0.315 eV and 0.426 eV respectively. These values were found to be in very good agreement with those calculated from relaxation peaks (0.329 eV for $MnFe_2O_4$ and 0.412 eV for $Mn_{0.8}Zn_{0.2}Fe_2O_4$). The high values of activation energy are indicative of a polaron conduction as suggested earlier [31]. The activation energy is found to be increasing with zinc substitution.

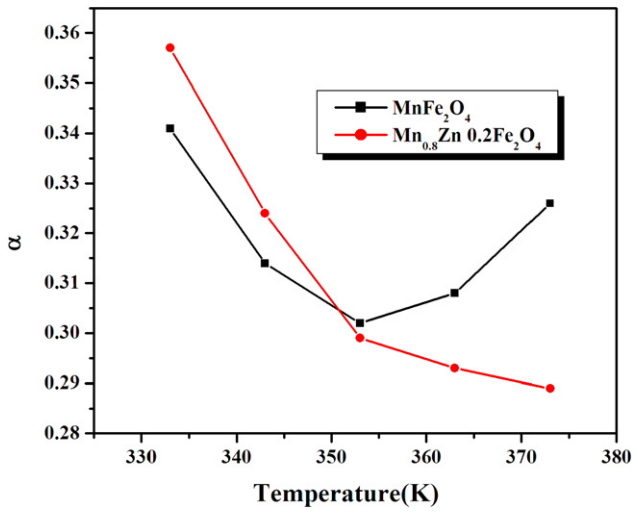


**Figure 28.** Variation of $\alpha$ with temperature.

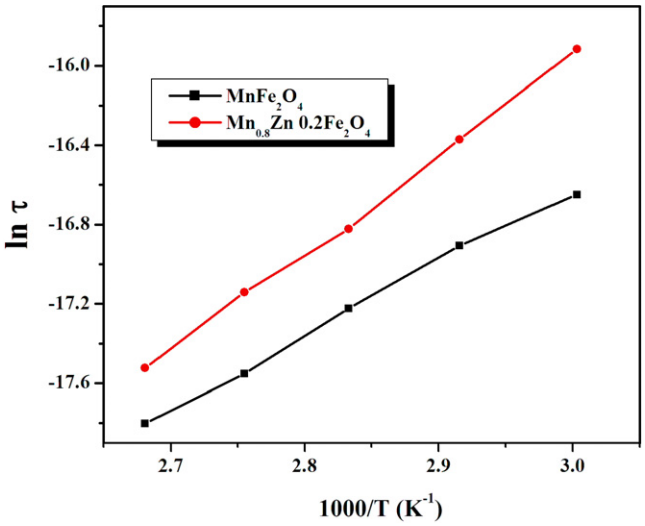


**Figure 29.** $\ln \tau$ versus $1000/T$.

## 4. Conclusions

The frequency and temperature dependence of the dielectric parameters of $Mn_{1-x}Zn_xFe_2O_4$ nanoparticles were studied. The low frequency dielectric dispersion was explained in terms of the Maxwell–Wagner theory of interfacial polarization. The effect of grains and grain interfaces was found to be enhanced in the nanoregime. The mechanism of dielectric polarization was found to be similar to that of the conduction process involving the hopping/tunneling of charge carriers. The decrease in $\varepsilon$ and $\varepsilon''$ with zinc substitution point to the decrease in availability of $Mn^{2+}$–$Mn^{3+}$ and $Fe^{2+}$–$Fe^{3+}$ pairs with increasing zinc. $\tan\delta$ and $\varepsilon''$ exhibit strong relaxation peaks and relaxation time $\tau$ was estimated from these relaxations. The activation energy for dielectric relaxation determined from $\tau$ values suggested a conduction involving polaron hopping or tunneling. The presence of dielectric relaxation implies the existence of multiple relaxation processes occurring in the system. Signatures corresponding to the existence of multiple relaxation times were evident from the Cole–Cole plot. Cole–Cole plots provide dispersion parameters and their temperature dependence was also studied.

## Acknowledgments

EVG acknowledges Cochin University of Science and Technology for the Research Fellowship. IAA-O would like to thank the Sultan Qaboos University for the support under grant number IG-SCI-PHYS-07-05. MRA acknowledges AICTE, Government of India ('Centre for ferrofluids' file No 8023/RID/ RPS-73/2004-05 dated 29/03/2005) for the financial assistance. KAM thanks the University Grant Commission, Government of India for the financial assistance received under the UGC minor project.

## References

[1] Somiya S, Aldinger F, Claussen N, Spriggs R M, Uchino K, Koumoto K and Kaneno M 2003 *Handbook of Advanced Ceramics* vol 2 (London: Academic)
[2] Valenzuela R 1994 *Magnetic Ceramics* (Cambridge: Cambridge University Press)
[3] Yin Y and Alivisators A P 2005 *Nature* **437** 664
[4] Sun S, Murray C B, Weller D, Folks L and Moser A 2000 *Science* **287** 1989
[5] Chikazumi S 1997 *Physics of Ferromagnetism* (Oxford: Clarendon)
[6] Sakurai J and Shinjo T 1967 *J. Phys. Soc. Japan* **23** 1426
[7] Calvin S, arpenter E E, Ravel B and Harris V G 2002 *Phys. Rev.* B **66** 224405
[8] Fatemi D J, Harris V G, Chen M X, Malik S K, Yelon W B, Long G J and Mohan A 1999 *J. Appl. Phys.* **85** 5172
[9] Tang Z X, Chen J P, Sorenson C M, Klabunde K J and Hadjipanayis G C 1992 *Phys. Rev. Lett.* **68** 3114
[10] Debye P 1929 *Polar Molecules* (New York: Dover)
[11] Cole K S and Cole R H 1941 *J. Chem. Phys.* **9** 34
[12] Wagner K W 1913 *Ann. Phys.* **40** 817
[13] Koops C G 1951 *Phys. Rev.* **83** 121
[14] Meaz T M, Attia S M and Abo El Ata A M 2003 *J. Magn. Magn. Mater.* **257** 296
[15] Vishwanathan B and Moorthy V R K 1990 *Ferrite Materials: Science and Technology* (Berlin: Springer)
[16] Iwachi K and Ikeda Y 1986 *Phys. Status Solidi* a **93** 309
[17] Abdeen A M 1999 *J. Magn. Magn. Mater.* **192** 121
[18] Cullity B D 1978 *Elements of X-Ray Diffraction* 2nd edn (Philippines: Addison-Wesley)
[19] Razet A 1998 *Metrologia* **35** 143
[20] Daniel Veera V 1967 *Dielectric Relaxation* (London: Academic)
[21] Hill N E, Vaughan W E, Price A H and Mansel Davies 1969 *Dielectric Properties and Molecular Behavior* (London: Van Nostrand-Reinhold)
[22] Sagar S, Saravanan S, Suresh Kumar S, Venkatachalam S and Anantharaman M R 2006 *J. Phys. D: Appl. Phys.* **39** 1678
[23] Veena Gopalan E, Al-Omari I A, Malini K A, Joy P A, Sakthi Kumar D, Yoshida Y and Anantharaman M R 2008 *J. Magn. Magn. Mater.* at press (doi:10.1016/j.jmmm.2008.10.031)
[24] Nalwa H S 2004 *Encyclopedia of Nanoscience and Nanotechnology* vol 2 (Los Angeles: American Scientific Publishers) p 371
[25] Fang H, Chen B, Jiang K, Sha J, Jiao Z, Zhang Q and Zhang L 1995 *Phys. Status Solidi* b **192** K11
[26] Miles Z P A, West Phal W B and Von Hippel A 1957 *Rev. Mod. Phys.* **29** 279

[27] Rezlescu N and Rezlescu E 1974 *Phys. Status Solidi* a **23** 575
[28] Denecke Mellisa A, Gun Ber W, Buxbaum G and Kuske P 1992 *Mater. Res. Bull.* **27** 507
[29] Abo El Ata A M and Attia S M 2003 *J. Magn. Magn. Mater.* **257** 165
[30] Zaki H M 2005 *Physica* B **363** 232
[31] Veena Gopalan E, Malini K A, Saravanan S, Sakthi Kumar D, Yoshida Y and Anantharaman M R 2008 *J. Phys. D: Appl. Phys.* **41** 185005
[32] Mazen S A, Matawe F and Mansour S F 1997 *J. Phys. D: Appl. Phys.* **30** 1799
[33] Klinger M I 1975 *J. Phys. C: Solid State Phys.* **8** 3595